Magnetic field dependence of low-temperature specific heat in Sr$_2$RuO$_4$

K. Machida and M. Ichioka

Department of Physics, Okayama University, Okayama 700-8530, Japan
(Received 28 November 2007; published 22 May 2008)

The magnetic field (H) dependence of the Sommerfeld coefficient $\gamma(H)$ of the low-temperature specific heat in Sr$_2$RuO$_4$ is analyzed by numerically solving the microscopic Eilenberger equation. By taking account of the strong Pauli-paramagnetic effect, we find that $\gamma(H)$ exhibits a systematic change from a concave function $\sqrt{H}$ to a convex function $H^\alpha(\alpha > 1)$ at high fields when the orientation of the magnetic field is varied, explaining experimental results. The magnetization is found to be consistent with this behavior. This implies either singlet pairing or triplet pairing with the d vector locked in the basal plane. Based on this conclusion, we explain other properties of this compound.

I. INTRODUCTION

Superconductors are classified into two distinct groups, which are characterized by either spin-singlet or spin-triplet pairing of electrons forming the Cooper pairs. Almost all superconductors that include high T_c cuprates belong to the former group. To date, only a few examples of spin-triplet superconductivity have been encountered. In the heavy Fermion material UPt$_3$, triplet pairing has been firmly identified.[1–4] The observed multiple phase diagram in the field (H) versus temperature (T) plane of UPt$_3$, consisting of three phases, A, B, and C, is reasonably explained only in terms of triplet pairing. This situation is similar to superfluid ^{3}He where two subphases Anderson-Brinkman-Morel and Balian-Werthamer are identified in the pressure vs T plane.[5] A direct probe to detect the spin structure of a Cooper pair is the Knight shift experiment. Most of other probes obtain information only about the orbital part of the pairing symmetry. In addition to distinguishing the spin-singlet or spin-triplet pairings, Knight shift experiments are used to identify the orientation of the d vector, which describes the spin structure of the spin-triplet pairing. In fact, the NMR Knight shift has played a fundamental role in confirming theoretical predictions[4] of the parity in UPt$_3$.[6] To identify the direction of the d vector, it is particularly crucial to experimentally determine both the field direction where the Knight shift decreased below T_c and the field directions where it remained constant,[6] which is in accordance to theoretical predictions.[4]

Sr$_2$RuO$_4$ is a second promising candidate for triplet pairing superconductivity.[7] A variety of theoretical and experimental works have been devoted to establishing the pairing symmetry, but a decade after its discovery,[8] it is still difficult to identify the spin structure of Cooper pairs in this material, though the gap structure of the orbital part with line nodes is now established. In Sr$_2$RuO$_4$, the contributions by the orbital dependent superconductivity of the α, β, and γ bands have also been studied.[7]

As the most direct probe to detect the spin part of the parity, Knight shift experiments were performed by using various nuclei, such as ^{87}Sr, ^{101}Ru, ^{99}Ru, and ^{17}O. Invariance of the Knight shift has been reported for both field directions of the c and ab axes as low as $H = 200$ G.[9] This fails to confirm the spin direction of pairs, i.e., the orientation of the

d vector, since the Knight shift does not change below T_c for any field direction. This is usually explained by suggesting that the d vector is not pinned to any particular direction strongly enough and, hence, it undergoes a rotation to a direction perpendicular to the applied field even for a field magnitude as low as 200 G. However, there remains a possibility that the spin part of the Knight shift is even smaller than the estimate obtained from the linear extrapolation[10] in the K-χ plot (where K is the Knight shift and χ is the total spin susceptibility). In this case, since the NMR experiment cannot detect the spin structure of the Cooper pairs within the experimental resolution, spin-singlet pairing cannot be ruled out.

In this paper, we discuss the spin part of the pairing function. Recent phase-sensitive experiments by Nelson *et al.*,[11] Kidwingira *et al.*,[12] and Xia *et al.*[13] suggested chirality or odd parity within the ab plane in Sr$_2$RuO$_4$. These results contain information of the orbital part of the pairing function. However, the spin part, such as the d-vector direction, has not been determined. With regard to these experimental results, it is noted that in addition to investigating the p-wave pairing scenario, attempts have been made to formulate an explanation in terms of the singlet scenario, such as chiral d-wave pairing $(k_x \pm ik_y)\sin k_z c$ by Zutic and Mazin[14] or reasons other than the pairing symmetry by Mineev.[15] The appearance of a spontaneous magnetic field below T_c, which is observed by muon spin relaxation,[16] may be associated with time reversal symmetry breaking of the pairing symmetry. This can also be explained by a spin-singlet scenario, such as chiral d-wave pairing, as well as spin-triplet chiral p-wave pairing $k_x \pm ik_y$. Related to this chirality of the pairing, spontaneous magnetic fields and supercurrents are predicted at the edge or domain boundary in chiral p-wave superconductors. However, the expected magnitude of the spontaneous field is not observed in Sr$_2$RuO$_4$.[17] Therefore, while spin-triplet chiral p-wave symmetry is considered to be plausible for superconductivity of Sr$_2$RuO$_4$, the supporting evidence is not conclusive. Some experimental results are difficult to explain within the simple scenario of spin-triplet chiral p-wave pairing. As an example, in this paper, we discuss the anomalous field dependence of the low-temperature specific heat at high fields for $H \| ab$ in Sr$_2$RuO$_4$, in relation to the paramagnetic effect through the spin part of the pairing. The paramagnetic effect works for spin-singlet pairing or spin-triplet pairing

with the *d*-vector locked along the magnetic field direction. The orbital part of the pairing function does not significantly affect the high-field behavior of the specific heat by the paramagnetic effect. Thus, in this study, a simple form is used for the orbital part of the pairing function, i.e., *d* wave. However, this does not represent the actual *d*-wave symmetry for the orbital part of the pairing in Sr_2RuO_4.

In this work, we examine the parity of the spin part in Sr_2RuO_4, including the possibility of spin-singlet pairing, through analyzing the specific heat experiment by Deguchi *et al.*[18,19] for various *T* and *H*. There are several outstanding problems posed by this experiment. Making progress on these problems will provide clues as to the nature of the spin part. One of the most interesting questions is why the field dependence of the Sommerfeld coefficient, $\gamma(H) = \lim_{T \to 0} C/T$ (where *C* is the specific heat), in the field along the basal *ab* plane shows a convex behavior H^α ($\alpha > 1$) in spite of the existence of a line node gap. This behavior is odd because $\gamma(H)$ is expected to show a concave $\sqrt{H}$-like behavior due to line nodes, i.e., the so-called Volovik effect.[20] It is remarkable that the convex curve becomes a Volovik $\sqrt{H}$ curve with a concave curvature when the applied field direction is tilted by only a few degrees from the basal *ab*-plane [see inset (a) in Fig. 3]. In addition to analyzing the specific heat data,[19] we also examine the magnetization data[21] in a field. We explain these experiments based on the idea that a strong Pauli-paramagnetic effect is important in the basal *ab* plane physics of Sr_2RuO_4 and establish a consistent picture for the dependence of the superconductivity on the magnetic field direction.

After explaining our formulation of quasiclassical theory in Sec. II, we discuss the field-orientation dependence of H_{c2} in order to estimate the effective paramagnetic parameter at each orientation in Sec. III. We analyze the field-orientation dependence of the Sommerfeld coefficient $\gamma(H)$ in Sec. IV and examine the magnetization curve in Sec. V. In Sec. VI, after discussing the pairing of the superconductivity in Sr_2RuO_4, we give a summary.

II. QUASICLASSICAL THEORY INCLUDING PARAMAGNETIC CONTRIBUTION

In our study of the vortex states, we take account of the paramagnetic depairing effect due to the Zeeman splitting term $\mu_B B(\mathbf{r})$ in addition to the orbital depairing effect by the vector potential $\mathbf{A}(\mathbf{r})$. The flux density of the internal field is $B(\mathbf{r})$ and μ_B is the renormalized Bohr magneton. Therefore, the Hamiltonian is given by

$$\mathcal{H} - \mu_0 \mathcal{N} = \sum_{\sigma=\uparrow,\downarrow} \int d^3\mathbf{r}\, \psi_\sigma^\dagger(\mathbf{r}) K_\sigma(\mathbf{r}) \psi_\sigma(\mathbf{r})$$
$$- \int d^3\mathbf{r}_1 \int d^3\mathbf{r}_2 [\Delta(\mathbf{r}_1,\mathbf{r}_2)\psi_\uparrow^\dagger(\mathbf{r}_1)\psi_\downarrow^\dagger(\mathbf{r}_2)$$
$$+ \Delta^*(\mathbf{r}_1,\mathbf{r}_2)\psi_\downarrow(\mathbf{r}_2)\psi_\uparrow(\mathbf{r}_1)], \qquad (1)$$

with

$$K_\sigma(\mathbf{r}) = \frac{\hbar^2}{2m}\left(\frac{\nabla}{i} + \frac{2\pi}{\phi_0}\mathbf{A}\right)^2 + \sigma\mu_B B(\mathbf{r}) - \mu_0, \qquad (2)$$

the flux quantum ϕ_0, and $\sigma = \pm 1$ for up- and down-spin electrons. μ_0 is the chemical potential. We consider the pairing of up-spin and down-spin electrons, i.e., the spin configuration for which paramagnetic effect appears. This is the case of spin-singlet pairing or triplet pairing with the *d* vector parallel to the magnetic field.[22] The Fourier transformation of $\Delta(\mathbf{r}_1, \mathbf{r}_2)$ with respect to $\mathbf{r}_1 - \mathbf{r}_2$ is given by $\Delta(\mathbf{r})\phi(\mathbf{k})$, where $\mathbf{r} = (\mathbf{r}_1 + \mathbf{r}_2)/2$ is the center-of-mass coordinate of the Cooper pair and $\mathbf{k}$ is the relative momentum of the pair.

We calculate the properties of the vortex states by the quasiclassical Eilenberger theory in the clean limit.[23–29] This framework is valid when $k_F \xi \gg 1$ (where k_F is the Fermi wave number and ξ is the coherence length). This is satisfied for Sr_2RuO_4, where $k_F\xi \sim 500$ ($k_F \sim 0.753$ Å^{-1} in the γ band and $\xi_{ab} = 660$ Å).[7] The quasiclassical Green's functions $g(\omega_l + i\tilde{\mu}B, \mathbf{k}, \mathbf{r})$, $f(\omega_l + i\tilde{\mu}B, \mathbf{k}, \mathbf{r})$, and $f^\dagger(\omega_l + i\tilde{\mu}B, \mathbf{k}, \mathbf{r})$ are calculated in the vortex lattice state by the Eilenberger equation in the presence of the paramagnetic contribution,[30–33]

$$\{\omega_n + i\tilde{\mu}B + \mathbf{v}(\mathbf{k}_F)\cdot[\nabla + i\mathbf{A}(\mathbf{r})]\}f = \Delta(\mathbf{r})\phi(\mathbf{k})g,$$
$$\{\omega_n + i\tilde{\mu}B - \mathbf{v}(\mathbf{k}_F)\cdot[\nabla - i\mathbf{A}(\mathbf{r})]\}f^\dagger = \Delta^*(\mathbf{r})\phi^*(\mathbf{k})g, \qquad (3)$$

where $g = (1 - ff^\dagger)^{1/2}$, Re $g > 0$, Matsubara frequency $\omega_n = (2n+1)\pi T$, and $\phi(\mathbf{k})$ is the pairing function along the Fermi surface $\mathbf{k}$. The Fermi velocity $\mathbf{v}$ is scaled by $v_{F0} = \langle|\mathbf{v}|^2\rangle_{\mathbf{k}}^{1/2}$, where $\langle\cdots\rangle_{\mathbf{k}}$ indicates the Fermi surface average. The paramagnetic parameter is $\tilde{\mu} = \mu_B B_0 / \pi k_B T_c$. In Eq. (3) and thereafter, length, temperature, magnetic field, and energy are scaled by R_0, T_c, B_0, and $\pi k_B T_c$, respectively. Here, $R_0 = \hbar v_{F0}/2\pi k_B T_c$ and $B_0 = \hbar c/2|e|R_0^2$. When a magnetic field is applied along the *z* axis direction, in the symmetric gauge, the vector potential is given by $\mathbf{A}(\mathbf{r}) = \frac{1}{2}\overline{\mathbf{B}} \times \mathbf{r} + \mathbf{a}(\mathbf{r})$, where $\overline{\mathbf{B}} = (0,0,\overline{B})$ is a uniform flux density and $\mathbf{a}(\mathbf{r})$ is related to the internal field $\mathbf{B}(\mathbf{r}) = \overline{\mathbf{B}} + \nabla \times \mathbf{a}(\mathbf{r})$. The unit cell of the vortex lattice for the pair potential $\Delta(\mathbf{r})$ and quasiclassical Green's functions is given by $\mathbf{r} = s_1(\mathbf{u}_1 - \mathbf{u}_2) + s_2\mathbf{u}_2$, where $-0.5 \leq s_i \leq 0.5$ ($i=1,2$), $\mathbf{u}_1 = (a,0,0)$, and $\mathbf{u}_2 = (a/2, a_y, 0)$ with $a_y/a = 1/2$ for a square lattice. The unit cell contains a vortex.

The pair potential is self-consistently calculated by

$$\Delta(\mathbf{r}) = g_0 N_0 T \sum_{0 < \omega_n \leq \omega_{\text{cut}}} \langle\phi^*(\mathbf{k})(f + f^{\dagger*})\rangle_{\mathbf{k}}, \qquad (4)$$

with $(g_0 N_0)^{-1} = \ln T + 2T\sum_{0<\omega_n\leq\omega_{\text{cut}}}\omega_l^{-1}$. We use $\omega_{\text{cut}} = 20$. By calculating $\Delta(\mathbf{r})$ self-consistently, we obtain the dependence of the vortex core size on *H*. This self-consistency is necessary for a quantitatively valid estimate of $\gamma(H)$.

The vector potential for the internal magnetic field is also self-consistently determined by

$$\nabla \times (\nabla \times \mathbf{A}) = \nabla \times \mathbf{M}_{\text{para}}(\mathbf{r}) - \frac{2T}{\tilde{\kappa}^2}\sum_{0<\omega_n}\langle\mathbf{v}_F \text{ Im } g\rangle_{\mathbf{k}}, \qquad (5)$$

using the large Ginzburg-Landau parameter $\tilde{\kappa} = 20$. In the right-hand side of Eq. (5), we consider both the diamagnetic contribution of the supercurrent in the last term and the

contribution of the paramagnetic moment, $\mathbf{M}_{\mathrm{para}}(\mathbf{r})$ $=[0,0,M_{\mathrm{para}}(\mathbf{r})]$, with

$$M_{\mathrm{para}}(\mathbf{r}) = M_0 \left[\frac{B(\mathbf{r})}{\bar{B}} - \frac{2T}{\tilde{\mu}\bar{B}} \sum_{0<\omega_n} \langle \mathrm{Im}\{g\} \rangle_{\mathbf{k}} \right]. \quad (6)$$

The normal state paramagnetic moment is $M_0 = (\tilde{\mu}/\tilde{\kappa})^2 \bar{B}$ with $\tilde{\kappa} = B_0 / \pi k_B T_c \sqrt{8 \pi N_0}$, where N_0 is the density of states (DOS) at the Fermi energy in the normal state. The self-consistent calculation of internal fields by $\mathbf{a}(\mathbf{r})$ does not significantly affect the behavior of $\gamma(H)$.

We alternately solve Eqs. (3)–(6) and obtain self-consistent solutions as in previous works[26,27] for a given unit cell of the vortex lattice. The unit cell is divided to 41×41 mesh points, where we obtain the quasiclassical Green's functions, $\Delta(\mathbf{r})$, $M_{\mathrm{para}}(\mathbf{r})$, and $\mathbf{A}(\mathbf{r})$. When we solve Eq. (3) by the explosion method, we estimate $\Delta(\mathbf{r})$ and $\mathbf{A}(\mathbf{r})$ at arbitrary positions by an interpolation from their values at the mesh points and by the periodic boundary condition of the unit cell taking account of the phase factor due to the magnetic field.[24,26,27]

By using the Doria-Gubernatis-Rainer scaling,[34,35] we obtain the following relation between $\bar{B}$ and the external field H:

$$H = \left(1 - \frac{\tilde{\mu}^2}{\tilde{\kappa}^2} \right) [\bar{B} + \langle (B(\mathbf{r}) - \bar{B})^2 \rangle_{\mathbf{r}} / \bar{B}]$$
$$+ \frac{T}{\tilde{\kappa}^2 \bar{B}} \left\langle \sum_{0<\omega_n} \left\langle \tilde{\mu} B(\mathbf{r}) \mathrm{Im}\{g\} + \frac{1}{2} \mathrm{Re}\left\{ \frac{(f^\dagger \Delta + f \Delta^*)g}{g+1} \right\} \right. \right.$$
$$\left. \left. + \omega_l \mathrm{Re}\{g-1\} \right\rangle_{\mathbf{k}} \right\rangle_{\mathbf{r}}, \quad (7)$$

where $\langle \cdots \rangle_{\mathbf{r}}$ indicates the spatial average. The magnetization, $M(T,H) = \bar{B} - H$, includes both the diamagnetic and paramagnetic contributions.

The local density of states is given by $N(\mathbf{r},E)$ $=N_{+1}(\mathbf{r},E) + N_{-1}(\mathbf{r},E)$ with

$$N_\sigma(\mathbf{r},E) = \langle \mathrm{Re}\{g (\omega_l + i\sigma\tilde{\mu}B,\mathbf{k},\mathbf{r})|_{i\omega_l \to E+i\eta}\} \rangle_{\mathbf{k}}, \quad (8)$$

for each spin component $\sigma = \pm 1$. We typically use $\eta = 0.01$. The DOS $N(E)$ is obtained by calculating the spatial average of $N(\mathbf{r},E)$, i.e., $N(E) = \langle N(\mathbf{r},E) \rangle_{\mathbf{r}}$. The zero-energy DOS $N(E=0,H)$ is identified as the Sommerfeld coefficient $\gamma(H)$ in the specific heat at low T since $C = \gamma T \propto N(E=0)T$ at low T. If we normalize $N(E=0)$ and $\gamma(H)$ by their normal state values N_0 and γ_0, respectively, we obtain $N(E=0,H)/N_0$ $= \gamma(H)/\gamma_0$. In our calculation, $\gamma(H)$ is evaluated at low temperature, $T/T_c = 0.1$.

In previous works, we reported the behavior of $\gamma(H)$ for various pairing symmetries when the Pauli-paramagnetic contribution is negligible ($\tilde{\mu}=0$).[27–29] In the case of a quasi-two-dimensional (Q2D) Fermi surface, H_{c2} for $H \parallel ab$ is much higher than that for $H \parallel c$. Even in this case, as shown in Fig. 3 of Ref. 28 for s-wave pairing, scaled $\gamma(H)$ as a function of H/H_{c2} shows a similar field dependence. Thus,

we may roughly discuss the behavior of $\gamma(H)$ for any field orientation, scaling H by H_{c2} based on the results calculated for $H \parallel c$.

Recently, we reported the behavior of $\gamma(H)$ in the presence of a strong paramagnetic contribution.[33] When we cannot neglect the paramagnetic contribution, $\tilde{\mu}$ is a key parameter for analyzing $\gamma(H)$. Since paramagnetic pair breaking becomes effective at higher fields of the order of the Pauli limiting field, $H_p = \Delta_0 / \sqrt{2}\mu_B$ (where Δ_0 is the gap amplitude at $T=0$), the effective paramagnetic parameter is related to the ratio of the hypothetical orbitally limited upper critical field H_{c2}^{orb} to H_p, i.e., effectively $\tilde{\mu} \to \tilde{\mu} H_{c2}^{\mathrm{orb}}/B_0 \propto H_{c2}^{\mathrm{orb}}/H_p$ with H in units of H_{c2}^{orb}, because $\tilde{\mu} H/B_0 = (\tilde{\mu} H_{c2}^{\mathrm{orb}}/B_0)H/H_{c2}^{\mathrm{orb}}$. For a Q2D Fermi surface with the paramagnetic effect, the field-angle dependence of the effective paramagnetic parameter $\tilde{\mu}(\theta)$ comes through the factor $H_{c2}^{\mathrm{orb}}(\theta)$. This orbital-limited $H_{c2}^{\mathrm{orb}}(\theta)$ is sensitive to the field orientation for highly anisotropic systems, such as in the present layered material Sr_2RuO_4. H_p is a material-specific bulk parameter independent of the field orientation. This is evidenced by the nearly isotropic bulk susceptibility observed.[7] Therefore, in our simple estimation of $\gamma(H)$, instead of rotating magnetic fields, we analyze the change by the field orientation through the dependence of the effective paramagnetic parameter $\tilde{\mu}(\theta)$ on the tilting angle θ.

We study the field-orientation dependence of $\gamma(H)$, assuming the presence of a paramagnetic contribution. Our main purpose is to understand the high-field behavior of $\gamma(H)$ in Sr_2RuO_4, i.e., the systematic change from a concave function $\sqrt{H}$ to a convex function H^α ($\alpha > 1$) at high fields depending on the field orientation. In the case of a strong paramagnetic contribution, the high-field behavior near $H_{c2}(\theta)$ shows a similar behavior for different pairing symmetries, while the lower-field behavior reflects the details of the anisotropy of the gap function and Fermi surface structure. For simplicity, we use a two-dimensional (2D) cylindrical Fermi surface, $\mathbf{k} = k_F(\cos\psi, \sin\psi)$, with $0 \le \psi < 2\pi$ and assume the d-wave pairing function, $\phi(\mathbf{k}) = \sqrt{2} \cos 2\psi$, to take account of the line node contribution in Sr_2RuO_4. Our analysis does not represent that the d-wave pairing is realized in Sr_2RuO_4. The details of the orbital structure of the pairing function do not give rise to serious differences in the high-field behavior of $\gamma(H)$ near $H_{c2}(\theta)$, where the paramagnetic contribution is dominant.

III. EFFECTIVE PARAMAGNETIC PARAMETER AT EACH FIELD ORIENTATION

Before discussing $\gamma(H)$, we estimate the anisotropy parameter Γ and the effective paramagnetic parameter $\tilde{\mu}(\theta)$ through analyzing the field-orientation dependence of the observed $H_{c2}(\theta)$. A reduction of H_{c2} from H_{c2}^{orb} due to the paramagnetic effect is obtained by solving the Eilenberger equation as $H_{c2}(\tilde{\mu}) = H_{c2}^{\mathrm{orb}}/\sqrt{1+2.4\tilde{\mu}^2}$. This is originally derived in the dirty limit s-wave case,[36] but we confirm it to be valid numerically in the present clean limit d-wave case too, as seen from Fig. 1, where the calculated values are compared to this expression.
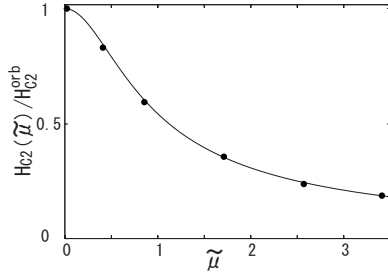
FIG. 1. Reduction of $H_{c2}(\tilde{\mu})$ as a function of $\tilde{\mu}$ evaluated by the quasiclassical Eilenberger equation (solid circles). The fitting curve is described by $H_{c2}(\tilde{\mu})/H_{c2}^{\rm orb}=1/\sqrt{1+2.4\tilde{\mu}^2}$ well.
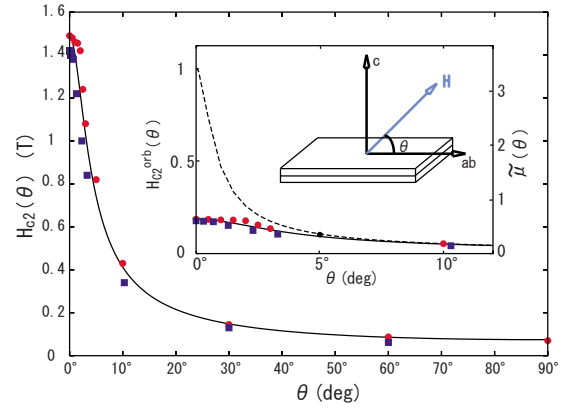

FIG. 2. (Color online) Calculated angle dependence of $H_{c2}(\theta)$ with $\Gamma=107$ and $\tilde{\mu}_0=3.41$ (solid line), where we assign $H_{c2\|ab}=1.45$ T. The circles (Ref. 19) and squares (Ref. 37) are experimental data. An enlarged figure is shown in the inset for small angles, plotting $H_{c2}(\theta)/H_{c2\|ab}^{\rm orb}$. The dashed line is the original orbital limit $H_{c2}^{\rm orb}(\theta)/H_{c2\|ab}^{\rm orb}$ of the effective mass form with $\Gamma=107$. The dashed line also shows $\tilde{\mu}(\theta)$ with $\tilde{\mu}_0=3.41$ (right-hand scale). θ is the angle from the ab plane.

It is natural to consider that $H_{c2}^{\rm orb}(\theta)$ is described by the effective mass model, namely, $H_{c2}^{\rm orb}(\theta)/H_{c2\|ab}^{\rm orb}=1/\sqrt{\Gamma^2 \sin^2 \theta+\cos^2 \theta}$, which simply embodies the fact that the orbital motion of electrons is determined by the directional cosine of the field to the basal plane. That is, $H_{c2}^{\rm orb}(\theta)\sim \phi_0/2\pi\xi_{ab}\xi_{\theta+90°}$, where $\xi_{\theta+90°}$ is the coherence length in the $\theta+90°$ direction, perpendicular to the magnetic field within the ac plane, and given by

$$\xi_{\theta+90°} \sim \hbar\langle v_{F\|\theta+90°}^2\rangle^{1/2}/k_B T_c$$
$$= \hbar(\langle v_{F\|ab}^2\rangle\cos^2 \theta + \langle v_{F\|c}^2\rangle\sin^2\theta)^{1/2}/k_B T_c$$
$$\sim \xi_c\sqrt{\Gamma^2 \cos^2 \theta + \sin^2 \theta}.$$

$\langle v_{F\|\theta+90°}^2\rangle$ indicates the Fermi surface average of the square of the Fermi velocity component for the $\theta+90°$ direction. Since θ is the angle from the ab plane, $\theta=0$ for $H\|ab$ and $\theta=90°$ for $H\|c$. The anisotropy $\Gamma=H_{c2\|ab}^{\rm orb}/H_{c2\|c}^{\rm orb}=\xi_{ab}/\xi_c$ is an unknown parameter here. However, it is assigned by the requirement that the experimental $H_{c2}(\theta)$ be theoretically reproduced. Namely, once Γ is determined, the angle dependence of $H_{c2}(\theta)$ is automatically known through the angle dependence of the paramagnetic parameter $\tilde{\mu}(\theta)$, which controls the reduction of the upper critical field H_{c2} from the "hypothetical" orbital-limited field $H_{c2}^{\rm orb}$.

Knowing the paramagnetic depairing effect on $H_{c2}(\tilde{\mu})$, we can calculate the angle dependence of the observed $H_{c2}(\theta)$ taking account of the fact that $\tilde{\mu}\propto H_{c2}^{\rm orb}/H_p$ has a θ dependence through the factor $H_{c2}^{\rm orb}(\theta)$ given above. Thus, we obtain $\tilde{\mu}(\theta)=\tilde{\mu}_0/\sqrt{\Gamma^2 \sin^2 \theta+\cos^2 \theta}$, where $\tilde{\mu}_0$ is the value at $\theta=0$. This θ dependence of $\tilde{\mu}(\theta)$ is crucial for explaining the anomalous θ dependence in the high-field behavior of the specific heat in Sr$_2$RuO$_4$, as will be discussed in Sec. IV.

By combining these relations, we finally obtain the θ dependence of the observed $H_{c2}(\theta)$ as $H_{c2}(\theta)=H_{c2\|ab}^{\rm orb}/\sqrt{\Gamma^2 \sin^2 \theta+\cos^2 \theta+2.4\tilde{\mu}_0^2}$. This takes account of both orbital and paramagnetic depairing effects. To reproduce the observed anisotropy $\Gamma^{\rm obs}\equiv H_{c2}(\theta=0)/H_{c2}(\theta=90°)=20$, we take $\tilde{\mu}_0=3.41$ when $\Gamma=107$. Note that $\tilde{\mu}_0$ and Γ are not independent parameters. As shown in Fig. 2, our effective mass model with the paramagnetic effect explains the angle dependence of $H_{c2}(\theta)$,[19,37] if one adjustable parameter is fixed. It should be noted, as shown in inset of Fig. 2, that the $\tilde{\mu}(\theta)$ value is completely determined by the effective mass form with $\Gamma=107$.

With regard to the assigned $\Gamma=107$, we note that the diamagnetic orbital current is determined by the perpendicular component of the average Fermi velocity to the field direction. Thus, Γ is the anisotropy ratio of the Fermi velocities, namely, $\Gamma=\sqrt{\langle v_{F\|c}^2\rangle/\langle v_{F\|ab}^2\rangle}$. This quantity is determined directly by de Haas-van Alphen experiment giving $\Gamma_\alpha=117$, $\Gamma_\beta=57$, and $\Gamma_\gamma=174$ for the three bands α, β, and γ, respectively.[7] Note that a simple arithmetic average $\Gamma_{\rm eff}=\frac{1}{3}(\Gamma_\alpha+\Gamma_\beta+\Gamma_\gamma)=116$ compares well with our assignment of $\Gamma=107$. There are virtually no adjustable parameters in our analysis. In passing, we note that the observed ratio, $\Gamma^{\rm obs}=H_{c2\|ab}/H_{c2\|c}=20$, is strongly reduced from $\Gamma_{\rm eff}$, apparently suggesting a reduction mechanism. We clarify this point in Sec. IV.

IV. FIELD DEPENDENCE OF LOW-TEMPERATURE SPECIFIC HEAT

We next discuss the specific heat at low T. In Fig. 3, we display $\gamma(H)$ for several values of $\tilde{\mu}$ together with the experimental data in inset (a) for various θ values. They show strikingly similar behaviors as a whole. The larger angle data exhibit a strong upward curvature, corresponding to the conventional $\gamma(H)\sim\sqrt{H}$, which is characteristic of a line node gap structure. This behavior is reproduced in our $\tilde{\mu}=0.02$ and 0.41 curves. As θ decreases, this changes to an almost linear relation for moderate H and forms a convex curve near H_{c2}. This behavior is reproduced by theoretical calculations for larger $\tilde{\mu}$. Thus, the overall "metamorphosis" of $\gamma(H)$ from conventional $\sqrt{H}$ to a strong convex curve is reproduced by increasing $\tilde{\mu}$. The main purpose of this study is to understand the high-field behavior of $\gamma(H)$.

As shown in inset (b) of Fig. 3, the data are fitted well by our calculations near H_{c2}, where we have used the $\tilde{\mu}(\theta)$ values determined above (see the inset of Fig. 2 with $\tilde{\mu}_0=3.41$). We have computed the six cases of $\tilde{\mu}$ shown in Fig. 3 and
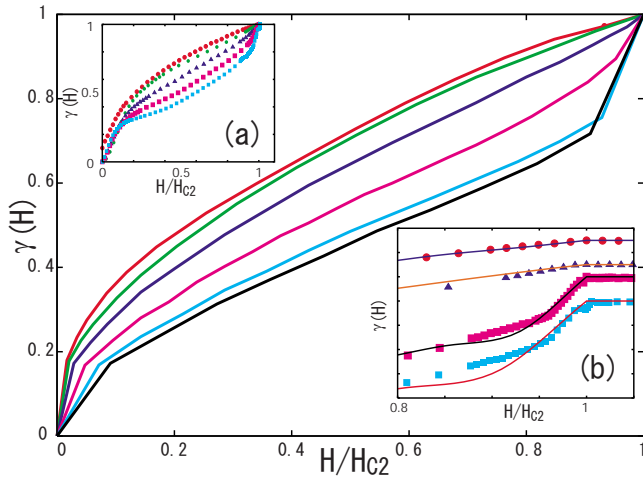
FIG. 3. (Color online) Zero-energy DOS $\gamma(H)$ at $T=0.1T_c$ for $\tilde{\mu}=0.02, 0.41, 0.86, 1.71, 2.57$, and 3.41 from top to bottom. We plot $\gamma(H)/\gamma_0$ as a function of H/H_{c2}. Inset (a) shows the experimental data (Ref. 19) for $\theta=0°, 2.5°, 3.0°, 5.0°$, and $90°$ from bottom to top. Inset (b) shows fits to the data for $\theta=0°$ by $\tilde{\mu}=3.41$, $0.5°$ ($\tilde{\mu}=2.36$), $5°$ ($\tilde{\mu}=0.33$), and $90°$ ($\tilde{\mu}=0.03$) from bottom to top, shifted upward.

obtained $\gamma(H)$ for other $\tilde{\mu}$ values by interpolation.

In Fig. 4, we display the theoretical behaviors of $\gamma(H)$ (a) and the corresponding specific heat data[19] (b), with $\tilde{\mu}(\theta)$ taken from the inset of Fig. 2. Our theoretical curves explain the data consistently. Of particular note is that (1) at $\theta=0°$, where $\tilde{\mu}(0)=\tilde{\mu}_0=3.41$ is largest, $\gamma(H)$ in our theoretical calculation shows a $\sqrt{H}$-like sharp rise in the small H region because of the presence of line nodes. However, this behavior is limited to only low fields. In the experimental data, $\gamma(H)$ shows a rapid increase below $H<0.15$ T. This is considered to be due to the contribution of the passive superconductivity of the α and β bands surviving only at low fields,[18,19] whose contributions are not included in our calculation. (2) In the intermediate field region (0.5 T$<H$ <1 T), $\gamma(H)$ exhibits an almost linear change with H. This extended linear change is shown to be thermodynamically consistent with the magnetization $M(T,H)$ behavior, as will be explained in Sec. V. (3) In the high-field region ($H>1$ T) toward $H_{c2}=1.45$ T, $\gamma(H)$ displays a sharp rise with a strong convex curvature. As H increases, the Pauli effect, which is linearly proportional to H, becomes increasingly effective, modifying $\gamma(H)$ from the usual $\sqrt{H}$ behavior to a convex H^α-like curve with $\alpha>1$.
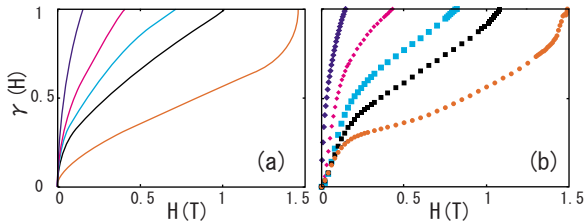

FIG. 4. (Color online) (a) $\gamma(H)/\gamma_0$ for $\tilde{\mu}=3.41, 0.60, 0.36, 0.18$, and 0.06 from bottom to top. We assign $H_{c2\|ab}=1.45$ T. (b) Corresponding experimental data (Ref. 19) for $\theta=0°, 3°, 5°, 10°$, and $30°$.
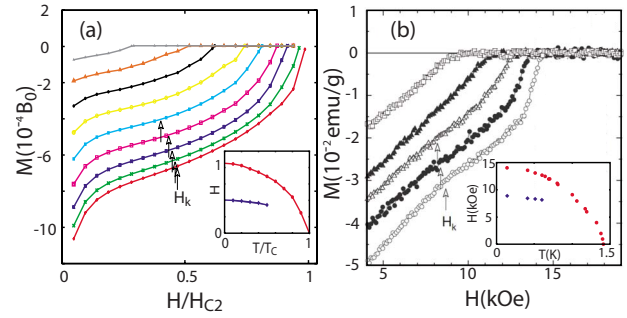

FIG. 5. (Color online) (a) Calculated magnetization curves for various $T/T_c=0.1, 0.2, 0.3, \ldots, 0.9$ from bottom to top when $\tilde{\mu}=1.71$ for $\theta=0°$. We plot $M(T,H)-M_0$ as a function of $H/H_{c2}(T=0.1T_c)$. The inset shows H_{c2} and the inflection point H_K. (b) Corresponding data (Ref. 21) for $T/T_c=0.1, 0.28, 0.40$, and 0.56 from bottom to top for $H\|ab$. The inset shows H_{c2} and the "kink" field H_K (Ref. 21). The magnetization M_0 of the normal paramagnetic moment is subtracted.

The data for $\theta=3°$ where $\tilde{\mu}(\theta=3°)=0.60$ show a similar behavior to that at $\theta=0°$, but the features associated with the Pauli effect, namely, the existence of an inflection point from concave to convex curves and a sharp rise toward H_{c2}, are weaker. The $\gamma(H)$ data for higher angles ($\theta>3°$) exhibit an intermediate behavior between those at $\theta=0°$ and the ordinary $\sqrt{H}$ curve, continuously changing their shapes with θ. It is remarkable that the highly convex curves of the experimental data at high fields for small angles, previously unexplained, are reproduced by the Pauli-paramagnetic effect. Physically, this effect makes the conventional Abrikosov vortex state unstable, ultimately leading to the normal state via a first order transition or the Fulde-Ferrell-Larkin-Ovchinnikov (FFLO) state. The sharp rise in $\gamma(H)$ near H_{c2} is a precursor to this.

V. FIELD DEPENDENCE OF MAGNETIZATION

Lastly, we discuss the magnetization curve $M(T,H)$ as a function of the magnetic field. In Fig. 5, we show the calculated results of magnetization $M(H)$ for several values of T (a) together with the experimental data[21] (b) to qualitatively understand the paramagnetic effects on $M(T,H)$. We do not attempt to quantitatively reproduce the data because the data are of a qualitative nature due to hysteresis effects. It is seen from Fig. 5(a) that the magnetization with a concave curvature at lower fields changes into a convex curvature toward H_{c2}. There is an inflection point field H_K at the change in curvature. The position of H_K decreases with T (see also insets). At higher T, H_K becomes invisible because of the thermal effect. These two features can be experimentally observed, as seen from the experimental data of $M(T,H)$ in Fig. 5(b). As shown in the insets, the inflection point field H_K roughly coincides with that for $\gamma(H)$, as seen from Fig. 4, implying that these are thermodynamically related.

As is seen from Fig. 5, as T decreases, the slope of $M(H)$ at H_{c2} becomes steeper, which means that the Maki parameter κ_2 decreases rather than increasing as in typical superconductors.[30,36] This is further clear supporting evi-

dence that the paramagnetic effect is important in Sr_2RuO_4.

It is easy to derive a thermodynamic Maxwell relation,

$$\frac{d}{dH}\frac{C}{T} = \frac{\partial^2}{\partial T^2}M(T,H), \qquad (9)$$

from which at low T we can see

$$\frac{\partial \gamma(H)}{\partial H} = \beta(H), \qquad (10)$$

with $M(T,H) = M_0(H) + \frac{1}{2}\beta(H)T^2$ at low T. To examine the relation of Eq. (10), we estimate $\beta(H)$ from the experimental data[21] in Fig. 5(b), finding that $\beta(H) \sim$ const for 0.5 T $< H < 1$ T. This implies that $\gamma(H) \propto H$ for this range of H. At higher fields around $H \sim 1.2$ T, since $\beta(H)$ has a curvature like that of H^3, we expect H^4-like behavior in $\gamma(H)$. These behaviors in $\gamma(H)$ are indeed seen for the $\theta = 0°$ data shown in Fig. 4. These analyses of $\gamma(H)$ and $\beta(H)$, which are free from any microscopic models, mean that the mysterious behavior of $\gamma(H)$ is thermodynamically intrinsic to the superconductivity in Sr_2RuO_4.

VI. DISCUSSION AND SUMMARY

Before presenting a summary, we will discuss the pairing symmetry and some related anomalous phenomena in Sr_2RuO_4. While the spin-triplet chiral p-wave symmetry is considered to be the most plausible pairing of Sr_2RuO_4, there are several known difficulties associated with this pairing symmetry.

(1) As mentioned above, experimentally, the superconductivity of Sr_2RuO_4 shows a strong suppression at high fields only when $H \| ab$. Thus, $\gamma(H)$ shows a convex curve H^α ($\alpha > 1$) near H_{c2}. This suppression can be explained by a strong paramagnetic effect, as discussed in this work. This is possible only for either singlet pairing or triplet pairing with the d vector locked in the basal plane because paramagnetic pair breaking occurs when Cooper pairs are formed between up-spin and down-spin electrons (with the direction of spin defined relative to the magnetic field direction). Thus, triplet states, such as $\hat{z}(p_x + ip_y)$ (Ref. 38) or $\hat{z}(p_x + ip_y)\cos p_z$,[39] cannot explain the paramagnetic effects because paramagnetic depairing does not occur when the d vector is not locked in the basal plane. This conclusion for the paramagnetic effect is not consistent with the Knight shift invariance below T_c if the NMR experiment is able to see the spin part within experimental accuracy.[9,10] The conclusion that the pairing symmetry of Sr_2RuO_4 is spin triplet and the d vector is always perpendicular to the magnetic field requires an alternative mechanism to explain the strong high-field suppression of superconductivity and the anomalous high-field behavior of $\gamma(H)$ for $H \| ab$.

(2) When the magnetic field is rotated within the ab plane, the anisotropy of the in-plane H_{c2} is experimentally very small, within a few percent of H_{c2}. Theoretically, however, two-component chiral p-wave pairing states usually give a large in-plane H_{c2} anisotropy,[15,40,41] which is not observed in Sr_2RuO_4. The present singlet scenario does not induce such large anisotropy. To obtain a small anisotropy

within chiral p-wave pairing, we need to choose the appropriate pairing function and to tune its detailed form.[41]

The origin of the convex behavior of $\gamma(H)$ near H_{c2} is the strong paramagnetic effect by the spin part of the Cooper pairs. Since the orbital part of the pairing does not significantly contribute to the high-field behavior of $\gamma(H)$, our analysis at high fields does not give information to identify the orbital part. We have used the d-wave pairing function for the orbital part as a simple example. However, this is not a definite identification of the orbital part in the pairing function of Sr_2RuO_4. Since the structure of the orbital part, such as the gap structure, affects the low-field behavior of $\gamma(H)$, further study is required on the orbital part to obtain a better fit of $\gamma(H)$ for the whole range of H.

Let us now consider the high-field phase for $H \| ab$ observed as a double transition.[37] This transition appears in a narrow H-T region along $H_{c2\|ab}$, starting at $T_0 = 0.8$ K or $T_0 = 0.53T_c$, at which point three transition lines meet, giving rise to a tricritical point in the H vs T plane. T_0 is remarkably similar to the so-called Lifshitz point $T_L = 0.56T_c$ in the FFLO phase diagram for a Pauli limited superconductor where the orbital depairing is completely quenched. This number, $T_L = 0.56T_c$, is universal, valid for a variety of situations, including three-dimensional Fermi sphere s-wave,[42] 2D s-wave,[43] d-wave,[44] and 1D s-wave[45] models. Our identified large paramagnetic parameter, $\tilde{\mu} = 3.41$, indicates that our system is almost Pauli limiting where the orbital effect is almost perfectly quenched because of the extreme two dimensionality in Sr_2RuO_4. We note that the identified anisotropy, $\Gamma = 107$, implies $H_{c2\|ab}^{orb} \sim 7.5$ T, which is reduced to $H_{c2\|ab} = 1.5$ T by the Pauli effect. Thus, we propose here to identify this high-field phase as FFLO.

The extreme two dimensionality is clear: if H is tilted away from the ab plane by as little as $\theta > 0.3°$, the double transition vanishes.[37] According to Nakai et al.,[46] the FFLO region at low T occupies a region $\sim 0.8\%$ below H_{c2}, which is comparable to the width of ~ 200 G of the high-field phase below $H_{c2\|ab} = 1.5$ T, a region of 200 G/1.5 T $\sim 1.3\%$.[37] Based on the known phase diagram,[36] we predict that as the field orientation θ increases, $\tilde{\mu}$ decreases and this high-field phase survives only for $0 < \theta < 0.3°$, quickly diminishing for $\theta > 0.3°$. At around $\theta \sim 1.0°$, a first order transition appears along the H_{c2} line instead of FFLO. It disappears for $\theta > 2.0°$, above which the paramagnetic effect becomes ineffective and Sr_2RuO_4 can be described as a conventional singlet superconductor with line nodes. These predictions based on our analysis are experimentally testable, although the details must be further theoretically sharpened.

In conclusion, we have analyzed both the specific heat at low T and the magnetization $M(T,H)$ by self-consistently solving the microscopic quasiclassical Eilenberger equation, including the contribution of the strong paramagnetic effect. It is seen that the Pauli-paramagnetic depairing effect is essential in understanding the experimental data in Sr_2RuO_2, especially to explain the high-field suppression of superconductivity when $H \| ab$. Considering the paramagnetic effect, we analyzed the change from a concave $\sqrt{H}$ behavior of the Sommerfeld coefficient $\gamma(H)$ to a convex H^α ($\alpha > 1$) behavior at high fields when the orientation of magnetic field is exactly aligned to $H \| ab$. This strong suppression of super-

conductivity by the strong paramagnetic effect is due to the spin part of the Cooper pairs and is possible only for singlet pairing or triplet pairing with the d vector locked in the basal plane. While the pairing symmetry of Sr_2RuO_4 is usually considered to be a spin-triplet chiral p-wave symmetry, there still exist anomalous behaviors which cannot be explained by a simple spin-triplet chiral p-wave symmetry scenario. Thus, to identify the pairing symmetry of Sr_2RuO_4, further careful study and analysis are necessary both in theoretical and experimental works.

[1] K. Machida, Prog. Theor. Phys. Suppl. **108**, 229 (1992).

[2] J. A. Sauls, Adv. Phys. **43**, 113 (1994).

[3] R. Joynt and L. Taillefer, Rev. Mod. Phys. **74**, 235 (2002).

[4] K. Machida, M. Ozaki, and T. Ohmi, J. Phys. Soc. Jpn. **58**, 4116 (1989); K. Machida and M. Ozaki, Phys. Rev. Lett. **66**, 3293 (1991); K. Machida, T. Nishira, and T. Ohmi, J. Phys. Soc. Jpn. **68**, 3364 (1999).

[5] A. J. Leggett, Rev. Mod. Phys. **47**, 331 (1975).

[6] H. Tou, Y. Kitaoka, K. Ishida, K. Asayama, N. Kimura, Y. Onuki, E. Yamamoto, Y. Haga, and K. Maezawa, Phys. Rev. Lett. **80**, 3129 (1998).

[7] A. P. Mackenzie and Y. Maeno, Rev. Mod. Phys. **75**, 657 (2003).

[8] Y. Maeno, H. Hashimoto, K. Yoshida, S. Nishizaki, T. Fujita, J. G. Bednorz, and F. Lichtenberg, Nature (London) **372**, 532 (1994).

[9] H. Murakawa, K. Ishida, K. Kitagawa, Z. Q. Mao, and Y. Maeno, Phys. Rev. Lett. **93**, 167004 (2004), and references cited therein.

[10] K. Ishida, H. Mukuda, Y. Kitaoka, Z. Q. Mao, H. Fukazawa, and Y. Maeno, Phys. Rev. B **63**, 060507(R) (2001).

[11] K. D. Nelson, Z. Q. Mao, Y. Maeno, and Y. Liu, Science **306**, 1151 (2004).

[12] F. Kidwingira, J. D. Strand, D. J. Van Harlingen, and Y. Maeno, Science **314**, 1267 (2006).

[13] J. Xia, Y. Maeno, P. T. Beyersdorf, M. M. Fejer, and A. Kapitulnik, Phys. Rev. Lett. **97**, 167002 (2006).

[14] I. Zutic and I. Mazin, Phys. Rev. Lett. **95**, 217004 (2005).

[15] V. P. Mineev, arXiv:cond-mat/0703624v2 (unpublished); Phys. Rev. B **76**, 212501 (2007).

[16] G. M. Luke, Y. Fudamoto, K. M. Kojima, M. I. Larkin, J. Merrin, B. Nachumi, Y. J. Uemura, J. E. Sonier, Y. Maeno, Z. Q. Mao, Y. Mori, H. Nakamura, and M. Sigrist, Nature (London) **394**, 558 (1998).

[17] See the recent result on this topic, J. R. Kirtley, C. Kallin, C. W. Hicks, E.-A. Kim, Y. Liu, K. A. Moler, Y. Maeno, and K. D. Nelson, Phys. Rev. B **76**, 014526 (2007).

[18] K. Deguchi, Z. Q. Mao, H. Yaguchi, and Y. Maeno, Phys. Rev. Lett. **92**, 047002 (2004).

[19] K. Deguchi, Z. Q. Mao, and Y. Maeno, J. Phys. Soc. Jpn. **73**, 1313 (2004).

[20] G. E. Volovik, JETP Lett. **58**, 469 (1993).

[21] K. Tenya, S. Yasuda, M. Yokoyama, H. Amitsuka, K. Deguchi, and Y. Maeno, J. Phys. Soc. Jpn. **75**, 023702 (2006).

[22] For example, V. P. Mineev and K. V. Samokhin, *Introduction to Unconventional Superconductivity* (Gordon and Breach, Amsterdam, 1999), Sec. 2.

[23] G. Eilenberger, Z. Phys. **214**, 195 (1968).

[24] U. Klein, J. Low Temp. Phys. **69**, 1 (1987).

[25] N. Schopohl, J. Low Temp. Phys. **41**, 409 (1980).

[26] M. Ichioka, N. Hayashi, and K. Machida, Phys. Rev. B **55**, 6565 (1997).

[27] M. Ichioka, A. Hasegawa, and K. Machida, Phys. Rev. B **59**, 184 (1999); **59**, 8902 (1999).

[28] M. Ichioka, K. Machida, N. Nakai, and P. Miranović, Phys. Rev. B **70**, 144508 (2004).

[29] M. Ichioka and K. Machida, Phys. Rev. B **65**, 224517 (2002).

[30] H. Adachi, M. Ichioka, and K. Machida, J. Phys. Soc. Jpn. **74**, 2181 (2005).

[31] U. Klein, D. Rainer, and H. Shimahara, J. Low Temp. Phys. **118**, 91 (2000).

[32] M. Ichioka, H. Adachi, T. Mizushima, and K. Machida, Phys. Rev. B **76**, 014503 (2007).

[33] M. Ichioka and K. Machida, Phys. Rev. B **76**, 064502 (2007).

[34] M. M. Doria, J. E. Gubernatis, and D. Rainer, Phys. Rev. B **41**, 6335 (1990).

[35] K. Watanabe, T. Kita, and M. Arai, Phys. Rev. B **71**, 144515 (2005).

[36] D. Saint-James, G. Sarma, and E. J. Thomas, *Type II Superconductivity* (Pergamon, Oxford, 1969), p. 171.

[37] K. Deguchi, M. A. Tanatar, Z. Q. Mao, T. Ishiguro, and Y. Maeno, J. Phys. Soc. Jpn. **71**, 2839 (2002).

[38] T. M. Rice and M. Sigrist, J. Phys.: Condens. Matter **7**, L643 (1995).

[39] Y. Hasegawa, K. Machida, and M. Ozaki, J. Phys. Soc. Jpn. **69**, 336 (2000).

[40] K. Machida, T. Ohmi, and M. Ozaki, J. Phys. Soc. Jpn. **54**, 1552 (1985).

[41] R. P. Kaur, D. F. Agterberg, and H. Kusunose, Phys. Rev. B **72**, 144528 (2005).

[42] S. Takada and T. Izuyama, Prog. Theor. Phys. **41**, 635 (1969).

[43] H. Shimahara, Phys. Rev. B **50**, 12760 (1994).

[44] A. B. Vorontsov, J. A. Sauls, and M. J. Graf, Phys. Rev. B **72**, 184501 (2005).

[45] K. Machida and H. Nakanishi, Phys. Rev. B **30**, 122 (1984).

[46] N. Nakai *et al.* (private communication).